Light Emitting Diodes (LED)

We have seen that if all the loss mechanisms are considered, the light extraction efficiency comes out to be very low (1 - 2 %). Following steps are taken to reduce photon losses (or improve photon extraction):

(1) To recover part of photons traveling towards the bottom contact.

There are various ways to achieve this. One may be to have a reflecting contact. This invariably results in poor electrical characteristics; due to increased ohmic voltage drop (contact resistance x current)

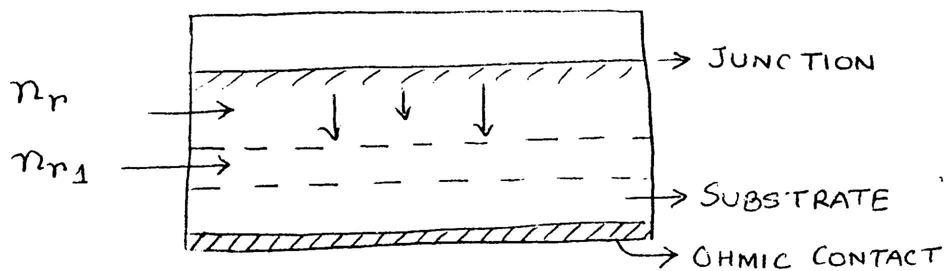

Figure 1.

Another way is to incorporate a layer, shown dotted in Fig. 1, having a lower index of refraction than the layer in which photons are generated.

$n_{r1} < n_r$

This would result in reflection: [For normal incidence]

$$R = \left[\frac{n_r - n_{r1}}{n_r + n_{r1}}\right]^2$$

So, $\frac{1}{2} I_0 R$ will be reflected up.

[For oblique incidence, relation is different]

(2) Increase critical angle θ_C to improve T
[$T = 1 - \cos\theta_C$]

$$\theta_c = Sin^{-1}\frac{n_{air}}{n_r}$$

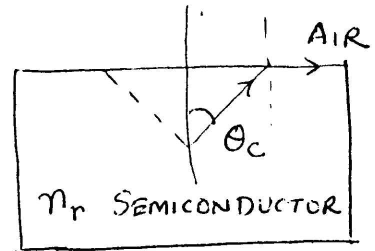

Fig. 2 (a)

$n_{r3} < n_r$

But, $n_{r3} > n_{air}$

$$\theta_c' = Sin^{-1}\frac{n_{r3}}{n_r}$$

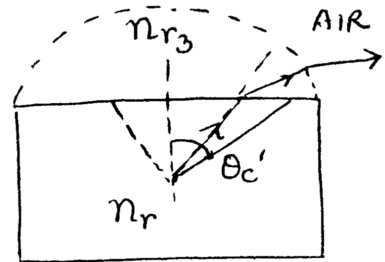

Fig. 2 (b)

Thus, $\theta_C' > \theta_C$

Hence, $T' = (1 - \cos\theta_C') > T$

The *dome shape* helps in reducing total internal reflections at the dome/air boundary.

(3) Reduce reflections from the *semiconductor/air* interface.

$$R = \left[\frac{n_r - n_{air}}{n_r + n_{air}}\right]^2$$

$$T = 1 - \left[\frac{n_r - n_{air}}{n_r + n_{air}}\right]^2 = \frac{4 n_r n_{air}}{(n_r + n_{air})^2}$$

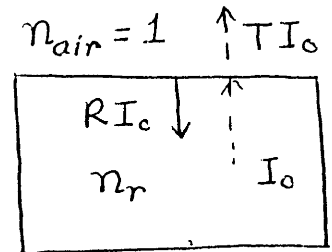

Fig. 3(a)

Using $n_{air} = 1$,

$$T = \frac{4 n_r}{(n_r + 1)^2}$$

same as in notes.

Solution: Insert or deposit an antireflection (AR) coating.

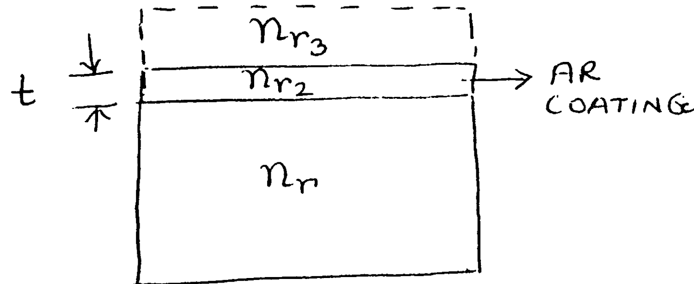

Fig. 3(b)

For the structure of Fig. 3(b),

$$R = \frac{(n_r n_{r3} - n_{r2}^2)^2}{(n_r n_{r3} + n_{r2}^2)^2} = \textit{Reflection coefficient}$$

- for normal incidence.

$$T = \frac{4 n_r n_{r3} n_{r2}^2}{(n_r n_{r3} + n_{r2}^2)^2}$$

$R = 0$, if $n_r n_{r3} = n_{r2}^2$

$$or,\ n_{r2} = \sqrt{n_r n_{r3}}$$

In addition, there is a phase condition:

$$n_{r2} * t = \frac{\lambda}{4}(2l - 1) \qquad l = 1,2,3,........(an\ integer)$$

That is, the thickness of the AR coating is multiple of $\lambda/4 * n_{r2}$.

Commonly used materials for antireflection coating:

SiO_2, SiO, TiO_2, ZrO_2, SiO_3N_4

$n_{r2} \simeq 1.8 - 1.9$

Finally, incorporating all the above improvements, we get,

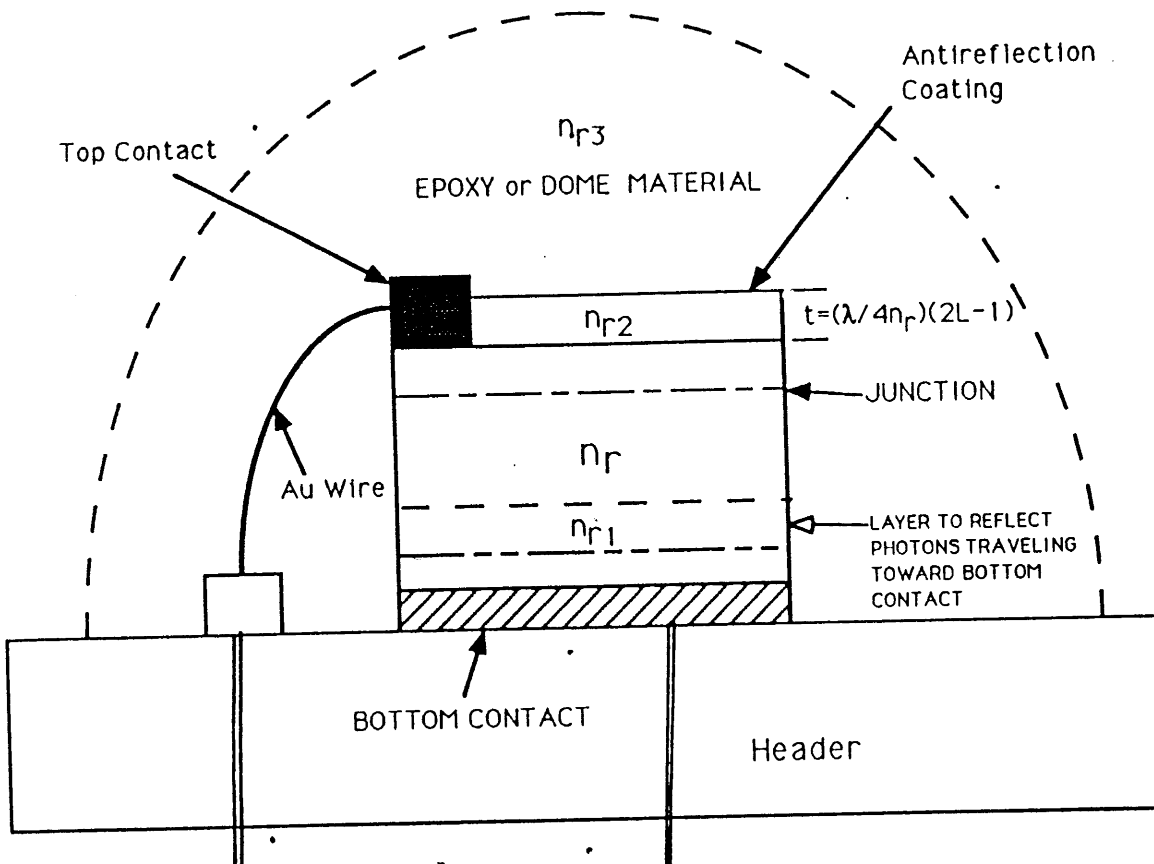

A typical LED chip on a TO 5 type header

(4) Heterojunctions: $(nAlGaAs - pGaAs)$

If the n-region is made using a wider energy gap material, this would result in small absorption in the window (or n-) region.

$$I(d) = I_0 e^{-\alpha d}$$

$$\alpha\,]_{\text{wider gap}} < \alpha\,]_{\text{narrow gap}} \quad , \text{for a given } h\nu \simeq E_g$$

Also η_{inj} is higher for heterojunctions.

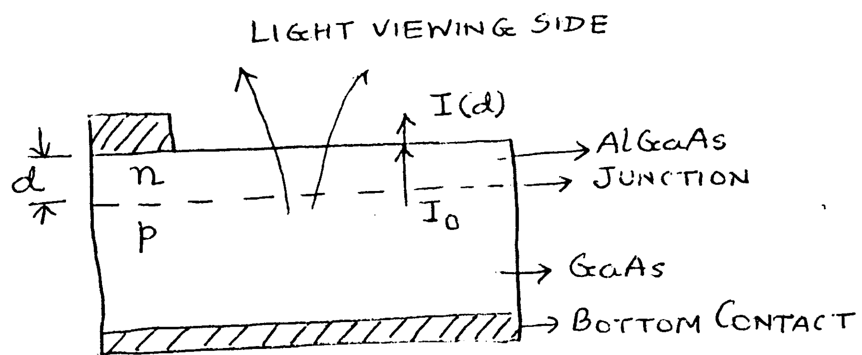

Fig. 4

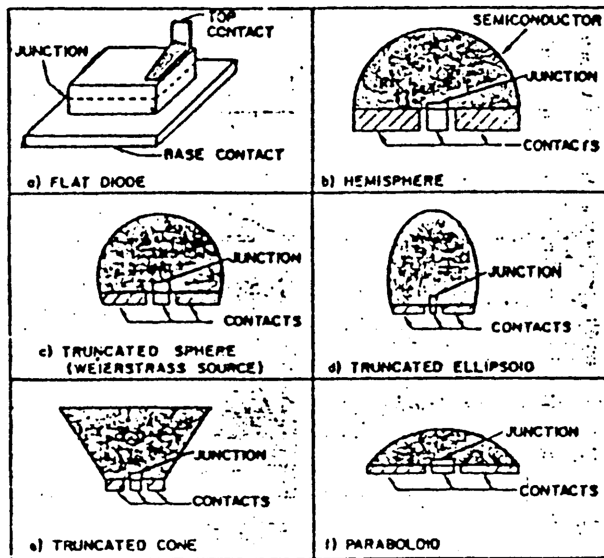

Fig. 14.7. LED geometries to increase the light extraction or optical efficiency. The effectiveness of the various geometries is listed in Table 14.1. (After Carr. Reprinted with permission from *Infrared Physics*, 6, 1966; © 1966 Pergamon Press.)

Table 14.1. Figures of Merit for Various LED Geometries per Unit Internal Light Flux Generation ($n = 3.6$)

Geometry	Radiant Flux	Maximum Radiant Intensity	Average Radiant Intensity
	P	$J(0)$ $\theta = 0$	$\langle J(0) \rangle$ $\theta = 26°$
Flat plane diode area emission	0.013	0.0042	0.0039
Hemisphere	0.34	0.054	0.054
Weierstrasse sphere	0.34	1.4	0.52
Truncated ellipsoid	0.25	9.8	0.39
Truncated cone	0.20	0.063	0.059
Paraboloid source			
$R_j/F_p = 0.1$	0.34	0.84	0.52
$R_j/F_p = 0.05$	0.34	3.3	0.52

(After Carr, reprinted from Infrared Physics, 1966, V. 6)

84I Inoshita, T.: J. Appl. Phys. **55** (1984) 2056.
84K Kobayashi, N., Fukui, T.: J. Cryst. Growth **67** (1984) 513.
84L Lai, S.T., Klein, M.V.: Phys. Rev. B **29** (1984) 3217.
84M Murawala, P.A.: Phys. Rev. B **29** (1984) 4807.
84R Radojewska, E.B., Bryskiewicz, T., Jedral, L., Brzezinski, J., Lewandow,ski, W.: Appl. Phys. Lett. **45** (1984) 988.
84W Wang, P.J., Wessels, B.W.: Appl. Phys. Lett. **44** (1984) 766.
85C Cohen, R.M., Cherng, M.J., Benner, R.E., Stringfellow, G.B.: J. Appl. Phys. **57** (1985) 4817.
85T Takeda, K., Matsumoto, N., Taguchi, A., Taki, H., Ohta, E., Sakata, M.: Phys. Rev. B **32** (1985) 1101.

Physical property	Numerical value	Experimental conditions	Experimental method, remarks	Ref.

2.16.3 Quaternary alloys of the type III_x–III_{1-x}–V_y–V_{1-y}

Quaternary alloys provide the possibility to grow epitaxial layers with a broad range of energy gaps lattice matched to a suitable substrate.

The condition for lattice matching can easily be derived from the interpolation scheme for the determination of a material parameter $P(x, y)$ for an alloy $A_xB_{1-x}C_yD_{1-y}$ from the same parameters of the four constituents:

$$P(x, y) = (1-x)\,y\,P(BC) + (1-x)(1-y)\,P(BD) + xy\,P(AC) + x(1-y)\,P(AD).$$

For lattice matching on substrate BD ($x = y = 0$) the condition $a(x, y) = a(BD)$ leads to

$$x = \frac{[a(BC) - a(BD)]\,y}{[a(BD) - a(AD)] - [a(BC) + a(AD) - a(BD) - a(AC)]\,y}$$

or, in a linear approximation to this formula – exact at $y = 0$ and $y = 1$:

$$x/y = [a(BC) - a(BD)]/[a(BC) - a(AC)].$$

The main interest in quaternary III–V alloys stems from the possible applications in micro- and optoelectronic devices. Thus most of the data in the following sections refer to quaternary alloys lattice matched to GaSb, InP and GaAs (see Fig. 1 in section 2.16.1). From the huge amount of papers on the characterization of quaternary layers and on device applications only the most important intrinsic data will be presented here.

The growth conditions are affected by the occurrence of miscibility gaps. We refer to basic discussions of these phenomena to [82S1, 83S1, 83S2].

Several types of quaternary alloys are possible:

(a) **III-III-V-V alloys.** These materials will be discussed in the following subsections.

(b) **III-III-III-V alloys.** Several systems will be presented in section 2.16.4.

(c) **III-V-V-V alloys.** Here only one system seems to be of interest for applications: $InAs_{1-x-y}Sb_xP_y$. We refer for this system to [80B, 81E. 82G1, 84A1].

Not much has been done in the field of *quintarnary alloys*. An example for such material is $(Al_xGa_{1-x})_{1-z}In_zP_yAs_{1-y}$ on GaAs [84M].

2.16.3.1 Gallium indium arsenide phosphide ($Ga_xIn_{1-x}As_yP_{1-y}$)

As shown in Fig. 1 of section 2.16.1 alloys of this system can be lattice matched on InP (E_g range: 0.73···1.35 eV), GaAs (E_g range: 1.42···1.90 eV) and ZnSe (slightly lower range). The matching conditions according to the formula above are ($0 \leq y \leq 1$):

x	$0.1894\,y/(0.4184 - 0.013\,y)$		on InP substrate	
	$\approx 0.47\,y$			
	$(1.00 + y)/2.08$		on GaAs substrate	
	$(1.06 + y)/2.06$		on ZnSe substrate	

Physical property	Numerical value	Experimental conditions	Experimental method, remarks	Ref.

Most data have been obtained for InP lattice matched samples. All data in the following tables and figures refer – if not stated otherwise – to InP lattice matched material.

The system has been reviewed in [82P1]. In [82A1] all relevant material parameters have been calculated from the corresponding parameters of the four binary constituents.

Electronic properties

direct energy gap (in eV):

Physical property	Numerical value	Experimental conditions	Experimental method, remarks	Ref.
$E_{g,dir}(x, y)$ ≃	$1.35+0.668x-1.068y+0.758x^2+0.078y^2-0.069xy-0.322x^2y+0.03xy^2$			84K1

from literature data for the constituents and interpolation formulas; for lattice match to InP this formula reduces to

Physical property	Numerical value	Experimental conditions	Experimental method, remarks	Ref.
$E_{g,dir}(y)$	$1.35-0.738y+0.138y^2$	RT	electroreflectance	80Y
	$1.350-0.883y+0.250y^2$	RT	electroreflectance	80P
	$1.35-0.775y+0.149y^2$	298 K	calculated, fitting photoluminescence and electroreflectance measurements, Fig. 1a [82P2]	82P2
	$1.425-0.7668y+0.149y^2$	4.2 K	calculated, fitting absorption and transmission measurements, Fig. 1b [82P2]	

The calculated compositional variation of $E_{g,dir}$ for GaAs and ZnSe lattice matched material is shown in Fig. 2 [82A1].

Theoretical approaches to $E_g(y)$: [81P2, 83P2].

bowing parameters for band gaps at L and X (in eV):

Physical property	Numerical value	Experimental conditions	Experimental method, remarks	Ref.
$c(\Gamma-L)$	0.10(5)		L-conduction band	84K2
$c(\Gamma-X)$	0.21(7)		X-conduction band from synchrotron radiation reflection spectroscopy	

higher interband transition energies (in eV):

Physical property	Numerical value	Experimental conditions	Experimental method, remarks	Ref.
E_1	$3.11+0.034x-0.885y+0.516x^2+0.275y^2-0.187xy+0.017x^2y$			80L

at RT, from fitting of literature data: for InP lattice matched material this formula reduces to

Physical property	Numerical value	Experimental conditions	Experimental method, remarks	Ref.
$E_1(y)$	$3.11-0.87y+0.30y^2+0.007y^3$	RT		80L
	$3.136-0.788y+0.222y^2$	RT		80P
	$3.14-0.739y+0.149y^2$	295 K	calculated, fitting electroreflectance and ellipsometric data, Fig. 3 [82P2]	82P2
	$3.163(13)-0.590(16)y+0.33(5)y^2$	RT	ellipsometry	82K2
$E_2(y)$	$5.04-0.309y+0.149y^2$	295 K	see also Fig. 4 [80L]	82P2
	$4.75-0.569y+0.149y^2$	295 K		81P1
$E'_0(y)$	$4.72(1)-0.31(2)y-0.01(5)y^2$	RT	ellipsometry	82K2

For further interband transition energies, see Fig. 4 [80L].

Physical property	Numerical value	Experimental conditions	Experimental method, remarks	Ref.
spin-orbit splitting energies (in eV):				
Δ_0 (y)	$0.119+0.300\,y$ $-0.107\,y^2$	RT	electroreflectance, see also Fig. 1 [82P2]	80P
Δ_1 (y)	$0.145+0.173\,y$ $-0.064\,y^2$		see also Fig. 5 [82P2]	80P
	$0.133(5)+0.124(7)\,y$ $-0.07(2)\,y^2$	RT	ellipsometry	82K2
effective masses (in units of m_0):				
m_n (x, y)	$0.08-0.116\,x+0.026\,y-0.059\,xy+(0.064-0.02\,x)\,y^2+(0.06+0.032\,y)\,x^2$			80R
interpolation formula; relations for InP lattice matched material are				
m_n (y)	$0.077-0.050\,y$ $+0.014\,y^2$	RT	Shubnikov – de Haas effect	80P
	$0.080-0.039\,y$		see also Fig. 6 [82P2]	80N

$m_{p,l}$: Fig. 7 [82P2], also [81H]
$m_{p,h}$, m_{so}: Fig. 8 [82A1].

Physical property	Numerical value	Experimental conditions	Experimental method, remarks	Ref.
electron g-factor:				
g_c	$1.35-2.47\,y-2.26\,y^2$	RT	electroreflectance	80P

Valence band parameters, hole-phonon coupling constants and alloy scattering potentials have been calculated for the full x, y range in [84T].

Lattice properties

The system of InP lattice matched alloys shows a miscibility gap (Fig. 9 [84K1]). For growth problems, see e.g. [82P1, 83Q, 84L], for phase diagrams and related problems, see [82G2, 83B, 84K1].

Physical property	Numerical value	Experimental conditions	Experimental method, remarks	Ref.
lattice parameter (in Å):				
a (x, y)	$5.8688-0.4176\,x$ $+0.1896\,y+0.0125\,xy$		linear interpolation from lattice parameters of four constituents	82A1

thermal expansion: Fig. 10 [82A1].

Physical property	Numerical value	Experimental conditions	Experimental method, remarks	Ref.
density (in g cm^{-3}):				
d	$5.477-0.712\,y$			82A1

hardness anisotropy: [84W1].

Experimental data on heat capacity and thermodynamic functions for the $(GaAs)_x(InP)_{1-x}$ system in the temperature range 4 K···300 K have been reported in [82S2].

phonon wavenumbers:

for InP lattice matched material: Fig. 11 [82L, 84I],
for GaAs lattice matched material: Fig. 12 [84I].
See also [86S] for Raman scattering data.

elastic moduli: Fig. 13 [82A1]. For respective figures of Young's modulus, bulk modulus, Poisson's ratio, anisotropy factor as well as sound velocities, see [82A1].

Transport properties

Mobility data have been reported in many papers on the characterization of epitaxial layers. We only show two typical diagrams: Fig. 14 [82H] for the electron mobility and Fig. 15 [82H] for the hole mobility.

Physical property	Numerical value	Experimental conditions	Experimental method, remarks	Ref.
Auger recombination in InP lattice matched materials:				
effective Auger coefficients in the formula $\tau^{-1} = An^2 + Bn$ (A in 10^{-29} cm^6 s^{-1}, B in 10^{-10} cm^{-3} s^{-1})				
A	1.5	x = 0.27	for Auger recombination, see also [82M, 85S]	84W2
	7.5	0.40		
	9.8	0.47		
B	1.2	0.27		
	1.0	0.40		
	0.4	0.47		

For electron and hole impact ionization coefficients, see e.g. [84O1, 83O2].

thermal resistivity: Fig. 16 [83A2].

Optical properties

refractive index:

Fig. 17 [82B2] for the range 0.3···1.1 μm; for $\lambda = 1.15$, 1.30 and 1.55 μm, see [84B2].

dielectric constant:

Physical property	Numerical value	Experimental conditions	Experimental method, remarks	Ref.
$\varepsilon(0)$	12.40 + 1.5 y		for photon energies up to E_g, see Fig. 18 [82A2]; calculated refractive indices in this range: [82A2, 83J]	82A2
$\varepsilon(\infty)$	9.55 + 2.2 y			

For electrooptic and photoelastic effects, see [83A1, 84A1, 84A2].

2.16.3.2 Gallium indium arsenide antimonide ($Ga_xIn_{1-x}As_ySb_{1-y}$)

This system is shown as shaded area in Fig. 1 of section 2.16.1. It is the only system applicable for the growth of low band gap epitaxial layers on GaSb substrate. In spite of interesting applications for optical sources and detectors in the 2···4 μm range only few reliable data on intrinsic properties have been published.

MBE layers (x = 0.75, y = 0.21) with an energy gap of about 0.69 eV have been investigated in [85T]. Various other compositions have been studied in [86C]. LPE growth is possible but meets difficulties by the existence of a miscibility gap (see [85T] and literature cited therein). For experimental and theoretical data on phase diagrams, see e.g. [82G2, 82K1, 83B], for optical and luminescence investigations, see [82B1, 84B1].

2.16.3.3 Aluminum gallium arsenide antimonide ($Al_xGa_{1-x}As_ySb_{1-y}$)

This system shows a broad miscibility gap. Epitaxial layer growth is possible

- *on GaSb* for small amounts of As; by adding small amounts of As the lattice matching of $Al_xGa_{1-x}Sb$ on GaSb can be improved (see Fig. 1 of section 2.16.1)
- *on GaAs* for small amounts of Sb; layers with y greater than 0.8 have been produced.

See [83P1] for phase diagrams and a literature review on epitaxial layers and optoelectronic applications.

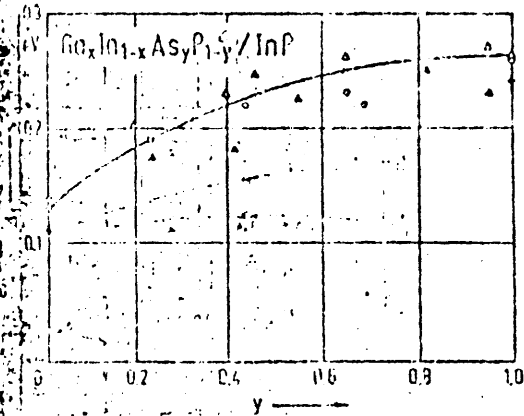

Fig. 5. $Ga_xIn_{1-x}As_yP_{1-y}$. Spin orbit splitting energy Δ_1 vs. composition for InP lattice matched material at 295K. Calculated curve and experimental data from four sources for ... [82P2].

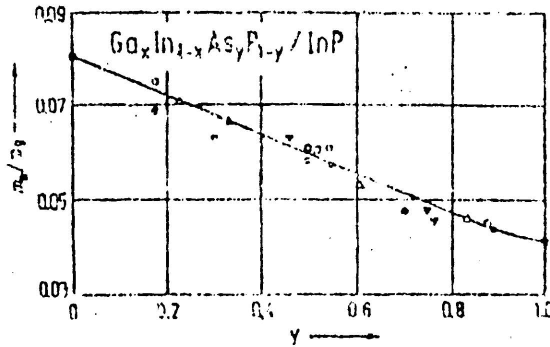

Fig. 6. $Ga_xIn_{1-x}As_yP_{1-y}$. Conduction band edge effective mass vs. composition for InP lattice matched material. Solid curve calculated from $k \cdot p$ theory, experimental data from six sources [82P2].

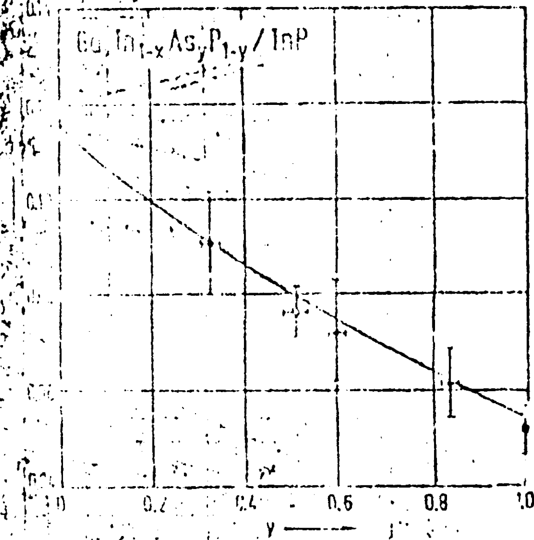

Fig. 7. $Ga_xIn_{1-x}As_yP_{1-y}$. Light hole effective mass vs. composition for InP lattice matched material. Solid curve calculated from $k \cdot p$ theory, experimental data at 2 K from four sources [82P2].

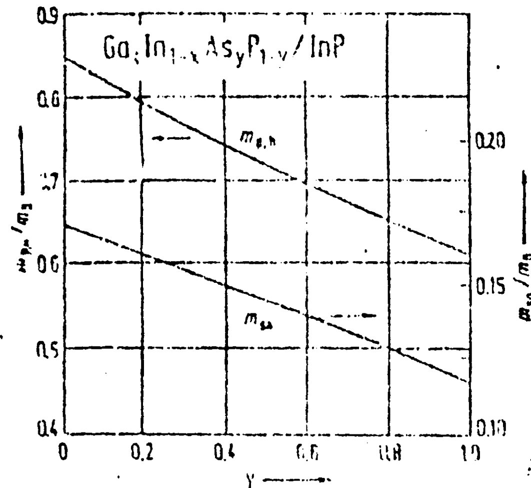

Fig. 8. $Ga_xIn_{1-x}As_yP_{1-y}$. Heavy hole mass and effective mass of the spin orbit split off valence band vs. composition for InP lattice matched material, calculated with an interpolation scheme [82A1].

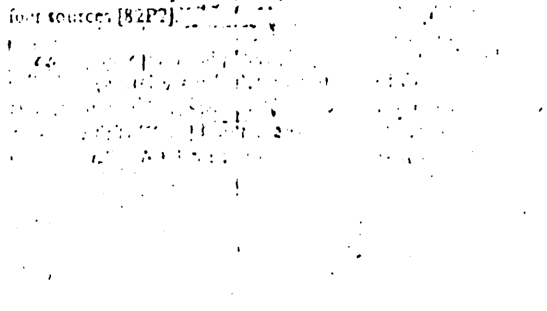

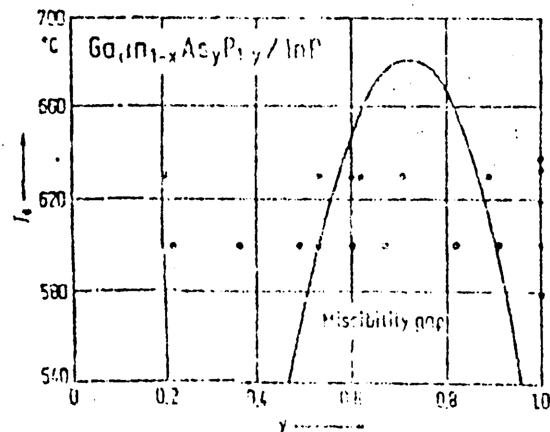

Fig. 9. $Ga_xIn_{1-x}As_yP_{1-y}$. Miscibility gap in InP lattice matched material (substrate temperature vs. composition). Spinodal curve calculated. Full circles: stable, open circles: unstable LPE layers [84K?].

Ref: Semiconductors: Intrinsic Properties of Group IV + III-V, II-VI, & I-VII Compounds
... Springer-Verlag 1987